Applied Physics Express **8**, 026501 (2015)
http://dx.doi.org/**10.7567/APEX.8.026501**

Laser sintering of silicon powder and carbon nanofibers for porous composite thick films

Yuki Iwabuchi and Jiwang Yan*

Department of Mechanical Engineering, Keio University, Yokohama 223-8522, Japan
E-mail: yan@mech.keio.ac.jp

Received October 27, 2014; accepted December 2, 2014; published online January 5, 2015

We attempted the laser sintering of a mixture of waste silicon powder from silicon wafer slicing processes and carbon nanofibers. Thick films with high porosity were successfully generated by a strong combination of silicon and carbon nanofibers. The surface porosity of the thick films and the crystallinity of silicon were controllable by varying the scanning speed of the laser beam. These findings indicate the feasibility of a new fabrication method for silicon anodes for future lithium-ion batteries. © 2015 The Japan Society of Applied Physics

High-capacity lithium-ion batteries are increasingly required in automobiles and portable electronic devices. The development of silicon anodes to replace conventional carbon electrodes has recently received attention.[1–3] The theoretical capacity of the conventional carbon material is 372 mAh/g, whereas that of silicon is 4,200 mAh/g, which is about 10 times higher.[4,5] Moreover, because the discharge potential of silicon is low, and the voltage change during discharge is small, silicon serves as a battery material for power supplies that can be used near their maximum capacities. However, volume expansion is a critical problem for silicon anodes. The volume expands by about 1.1 times during lithium-ion storage in conventional carbon anodes, but in a silicon anode, the volume expands by more than 3 times.[6] Thus, under repeated charge/discharge cycles, the silicon film on the current collector collapses and peels, causing the deterioration of the battery. As a result, the life of a silicon anode battery is shorter than that of a carbon anode battery.[7] To solve these problems, many studies have been conducted to develop new composite film anodes from silicon and carbon nanomaterials, such as carbon nanotubes.[8,9]

Conventional methods of fabricating composite films include chemical vapor deposition (CVD) and sputtering. However, these methods are relatively slow, and it is difficult to obtain a thick film. Sintering is an effective approach to thick-film fabrication, but conventional sintering processes using furnaces will cause thermal damage and deformation to the current collector substrates (copper films). To overcome these problems, in this study, we attempted to fabricate silicon/carbon composite thick films by laser sintering. Using a laser enables selective heating and sintering of thick films with less damage to the current collector substrates.[10,11] The processing efficiency of laser sintering is also higher than that of CVD and sputtering.

Another new proposal in this work is that, instead of using expensive silicon nanofibers or nanoparticles, we use waste silicon powder from the manufacturing processes of silicon wafers. In the manufacturing of solar cells and semiconductor substrates, especially the slicing of silicon ingots into silicon wafers, a large amount of silicon powder is generated with a particle size ranging from a few submicrons to a few microns.[12] Currently, more than half of the total volume of a silicon ingot is wasted as silicon powder. Because the waste silicon powder contains impurities, it cannot be reused for ingot production and is instead discarded as industrial waste. In recent years, other silicon wafer slicing technologies, such as that using atmospheric-pressure reactive microplasma,[13] have been developed, but have not been widely used in industry.

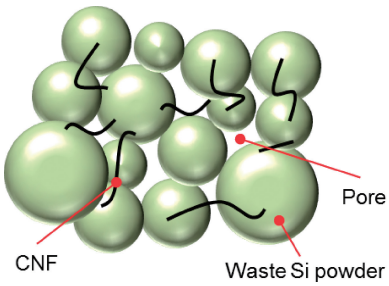

Fig. 1. Schematic model of Si/CNF composite film structure.

In this research, we attempted to reuse waste silicon powder for the production of Li-ion battery anodes to eliminate waste of energy and resources. To prevent electrode deterioration due to volume changes during the charge/discharge cycle, we tried to generate a porous structure in the thick film. Furthermore, we added carbon nanofibers (CNFs) to improve the electrical conductivity and mechanical strength of the electrodes. Figure 1 shows a schematic model of the target structure of the Si/CNF composite film. Laser sintering experiments were performed under various conditions, and the properties of the sintered carbon/silicon composite films were examined. The microstructure changes in the composite films during charge/discharge tests were also investigated.

To prepare the samples, waste silicon powder was mixed with CNFs (diameter: 10–20 nm; length: 0.1–10 μm; MD Nanotech Corporation) by a ball mill to obtain a slurry. N-methylpyrrolidone was added to the slurry as an organic solvent. The ratio of waste silicon powder to CNFs was 10 : 1 by mass. The mixed slurry was then applied to a 35-μm-thick copper film substrate as the current collector and dried at 60 °C.[14,15] Next, laser irradiation experiments were performed on the mixed powder. Table I shows the laser specifications and laser irradiation conditions. The resulting film thickness ranges from approximately 50 to 100 μm. The fabricated Si/CNF composite films were observed by scanning electron microscopy (SEM; Inspect S50) and field-emission SEM (FEI SIRION). Crystallinity analysis of silicon and CNFs was conducted by Raman spectrometry (JASCO NRS-3100) using a green laser with a wavelength of 532 nm.

Figure 2 shows a SEM micrograph of the boundary between a laser-irradiated region and an unirradiated region on a film surface. The laser fluence used was 7.7 mJ/cm^2. It is

Table I. Laser specifications and irradiation conditions.

Laser medium	Nd:YAG
Wavelength (nm)	532
Pulse width (ns)	15.4
Beam quality	TEM_{00}
Scanning speed (mm/s)	1–25
Scan interval (μm)	8–40
Beam diameter (μm)	240

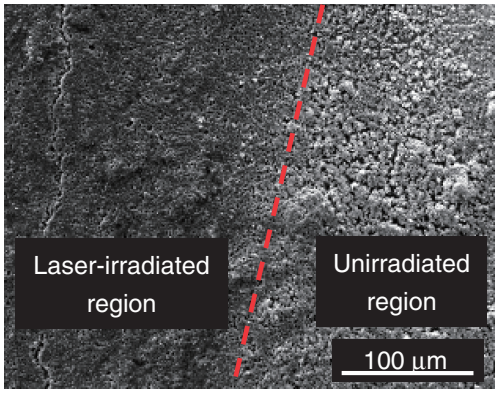

Fig. 2. SEM micrograph of a film surface showing boundary between laser-irradiated and unirradiated regions.

clear that in the unirradiated region, silicon particles are separate from each other, whereas after laser irradiation, the particles are combined, forming a porous structure.

The surfaces of thick films fabricated at various laser scanning speeds were compared. Figure 3(a) shows SEM micrographs of the film surfaces, where the scanning speed of the laser beam was varied from 5 to 25 mm/s. The film surfaces generally become smoother as the laser scanning speed increases. Figures 3(b) and 3(c) are higher magnification views of the film surfaces obtained at 5 and 25 mm/s, respectively. The surfaces are solid and almost no pores are seen in Fig. 3(b), whereas in Fig. 3(c), numerous pores are clearly seen. It can be assumed that at a low scanning speed, the silicon powder was completely melted and combined to form a solid structure; at a high scanning speed, however, silicon melting was incomplete, forming micropores.

The crystallinity of the films was analyzed using a laser Raman spectrometer. In Raman spectroscopy, a peak shift to the low-wave-number side indicates reduced crystallinity. For amorphous silicon, a broadband peak forms at around 470 cm^{-1}. As shown in Fig. 4, the waste silicon powder before laser irradiation has a peak at 502 cm^{-1}, indicating a polycrystalline or highly strained silicon structure. This is because in silicon slicing, chip formation involves material deformation and pulverization, which causes the polycrystallization of silicon.[16] However, after laser irradiation, the film has transitioned back to a structure close to that of single-crystal silicon (Raman shift: 520 cm^{-1}), as shown in Fig. 4. The improved crystallinity might be a result of the melting and recrystallization of the silicon powder during laser pulse application.

Figure 5 shows the peak shift and half-width of the films fabricated at various scanning speeds obtained by Raman mapping measurements. Figure 6 shows plots of the average

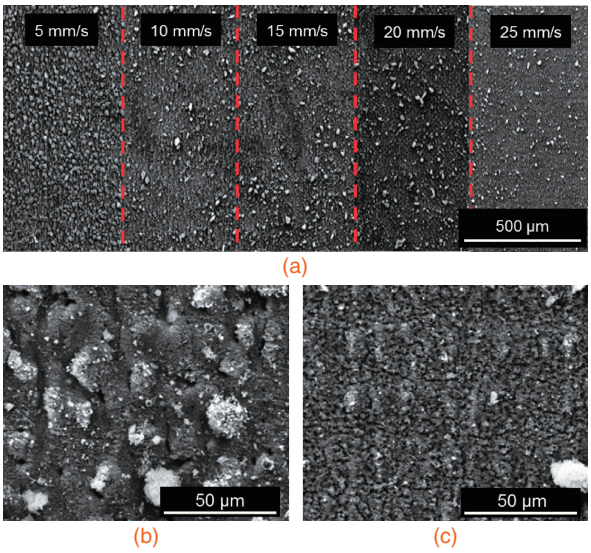

Fig. 3. (a) SEM micrographs of composite film surfaces obtained at various laser scanning speeds. (b) and (c) are magnified views at scanning speeds of 5 and 25 mm/s, respectively.

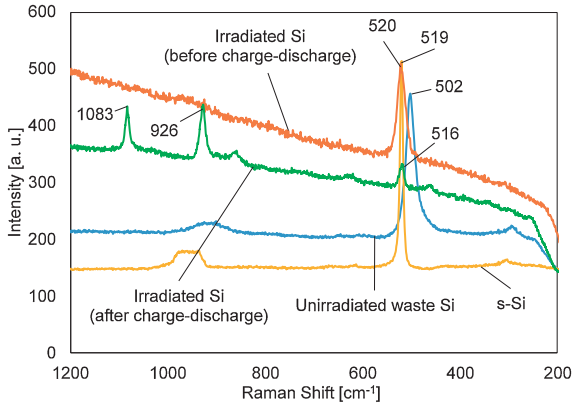

Fig. 4. Raman spectra of silicon particles under various processing conditions, with comparison to single-crystal silicon (s-Si).

half-width and peak shift at each laser scanning speed. The laser scanning speed clearly has little effect on the peak shift. On the other hand, the half-width increases with the scanning speed. It can be assumed that as the laser scanning speed increases, the time available for material heating and cooling decreases, and silicon recrystallization becomes incomplete. By changing the scanning speed of the laser beam, it may be possible to control the crystallinity of silicon, which is important for improving the absorption and desorption of lithium ions into and from silicon anodes.

To evaluate the mechanical performance of the fabricated Si/CNF composite films as a battery anode, pouch-type half-cells were fabricated, and charge/discharge tests were performed. The Si/CNF composite films were used as the working electrode, and Li metal foils were used as counter electrodes. The electrolyte used was 1.0 M $LiClO_4$ in 1 : 1 (v/v) ethylene carbonate/diethyl carbonate. The cells were cycled between 0.01 and 2.0 V at a current density of 0.27 mA/cm^2. Figure 7 shows SEM micrographs of the films after charge/discharge tests. Figure 7(a) is a film formed without laser irradiation, where many cracks are seen. Peeling of the film was observed in some other surface

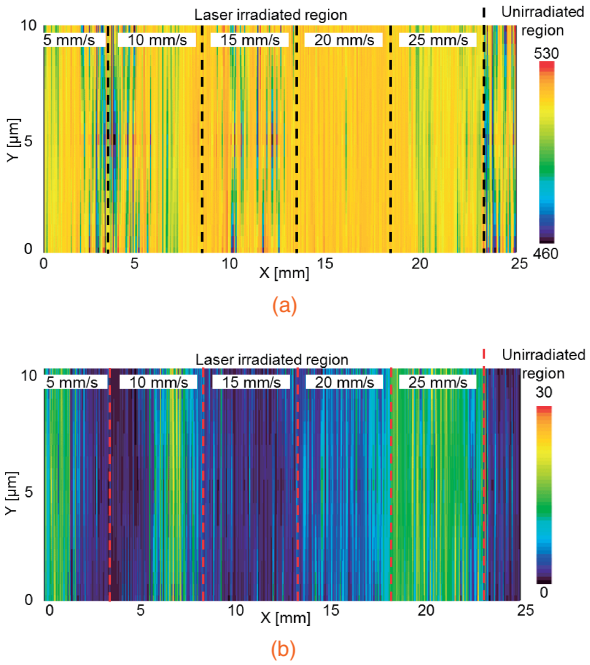

Fig. 5. Raman mapping measurements of (a) peak position and (b) half-width of films sintered at various laser scanning speeds.

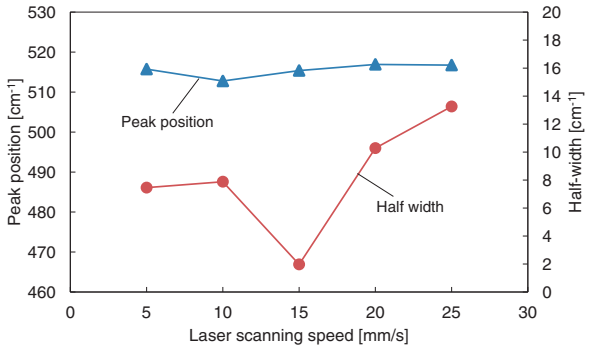

Fig. 6. Plots of average half-width and peak position at various laser scanning speeds.

regions. Figures 7(b)–7(d) show the films sintered at different laser scanning speeds (5–15 mm/s) and a laser fluence of 7.7 mJ/cm^2. In each case, the film surface became slightly rougher than that before the charge/discharge tests, indicating that the silicon powder partially collapsed because of the volume change. However, the films did not peel from the substrates, and no cracks appeared on the film surfaces. This result is attributed to the porous and network structures of Si and CNFs. The porous structure accommodates the volume change, and the network structure of Si and CNFs prevents the initiation and spread of cracks.

In addition, Raman spectroscopy analysis of the composite film was performed after the charge/discharge tests, and the result is also shown in Fig. 4. A few new Raman peaks of Si are seen from around 800 to 1100 cm^{-1}. These new peaks might be due to alloying of silicon with lithium during the charge/discharge tests, which is under further investigation.

In summary, we succeeded in fabricating composite thick films from waste silicon powder and CNFs by laser sintering. We realized a porous film structure and binding of Si and CNFs, which inhibit crack formation during the charge and

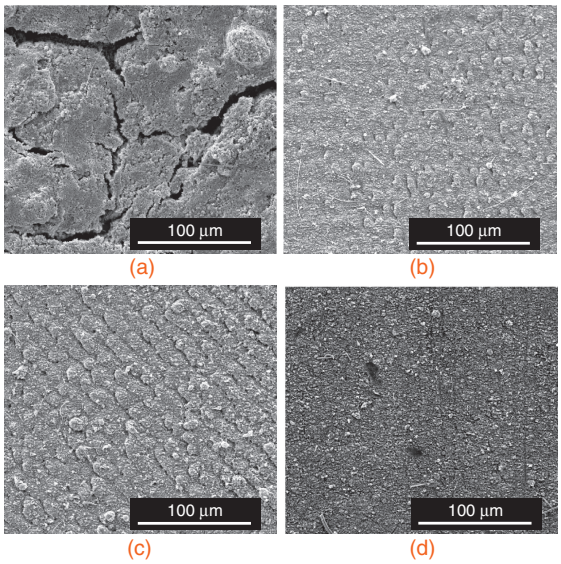

Fig. 7. SEM micrographs of various composite films after charge/discharge tests. (a) is a film without laser irradiation; (b), (c), and (d) are films sintered at laser scanning speeds of 5, 10, and 15 mm/s, respectively.

discharge of silicon anodes. The amount of Si melted, which affects film porosity, changes with the laser scanning speed. In addition, we confirmed that the silicon powder transitioned from a polycrystalline structure to a single-crystal structure during laser sintering, and the crystallinity depended on the laser scanning speed. These findings might contribute to the cost reduction and performance improvement of future lithium-ion batteries. The electrochemical properties of the composite thick films as battery anodes are under further investigation.

Acknowledgments The authors thank Professor Yasushi Katayama and Mr. Ryota Furuya of the Department of Applied Chemistry, Keio University, for their assistance in the charge/discharge tests.

1) M. Thakur, S. L. Sinsabaugh, M. J. Isaacson, M. S. Wong, and S. L. Biswal, Sci. Rep. **2**, 795 (2012).
2) S. R. Gowda, V. Pushparaj, S. Herle, G. Girishkumar, J. G. Gordon, H. Gullapalli, X. Zhan, P. M. Ajayan, and A. L. M. Reddy, Nano Lett. **12**, 6060 (2012).
3) H. Jung, M. Park, S. H. Han, H. Lim, and S. K. Joo, Solid State Commun. **125**, 387 (2003).
4) S. Hossain, Y. K. Kim, Y. Saleh, and R. Loutfy, J. Power Sources **114**, 264 (2003).
5) M. N. Obrovac, L. Christensen, D. B. Le, and J. R. Dahn, J. Electrochem. Soc. **154**, A849 (2007).
6) J. O. Besenhard, J. Yang, and M. Winter, J. Power Sources **68**, 87 (1997).
7) C. K. Chan, R. Ruffo, S. S. Hong, R. A. Huggins, and Y. Cui, J. Power Sources **189**, 34 (2009).
8) H. Habazaki, M. Kiriu, and H. Konno, Electrochem. Commun. **8**, 1275 (2006).
9) S.-L. Chou, Y. Zhao, J.-Z. Wang, Z.-X. Chen, H.-K. Liu, and S.-X. Dou, J. Phys. Chem. C **114**, 15862 (2010).
10) B. Duan and M. Wang, MRS Bull. **36**, 998 (2011).
11) B. Qian and Z. Shen, J. Asian Ceram. Soc. **1**, 315 (2013).
12) W. I. Clark, A. J. Shih, C. W. Hardin, R. L. Lemaster, and S. B. McSpadden, Int. J. Mach. Tools Manuf. **43**, 523 (2003).
13) T. Ideno, H. Inui, S. Takashima, H. Kano, M. Kondo, M. Hiramatsu, and M. Hori, Jpn. J. Appl. Phys. **47**, 5648 (2008).
14) L. F. Cui, L. Hu, J. W. Choi, and Y. Cui, ACS Nano **4**, 3671 (2010).
15) J. Y. Howe, D. J. Burton, Y. Qi, H. M. Meyer, III, M. Narzi, G. A. Narzi, A. C. Palmer, and P. D. Lake, J. Power Sources **221**, 455 (2013).
16) J. Yan, X. Gai, and T. Kuriyagawa, J. Nanosci. Nanotechnol. **9**, 1423 (2009).